공학석사학위논문

Evaluation of Stacking Fault Energy in Anisotropic FCC Metal by Nanoindentation

나노 압입을 통한 이방성 FCC 금속에서의 적층결함에너지 평가

2016년 2월

서울대학교 대학원

재료공학부

고 지 연

Evaluation of Stacking Fault Energy in Anisotropic FCC Metal by Nanoindentation

나노 압입을 통한 이방성 FCC 금속에서의 적층결함에너지 평가

지도교수 한 흥 남

이 논문을 공학석사학위논문으로 제출함

2016년 2월

서울대학교 대학원
재료공학부
고 지 연

고지연의 석사학위논문을 인준함
2015년 12월

위 원 장 유 웅 열 (인)

부 위 원 장 한 흥 남 (인)

위 원 박 은 수 (인)

ABSTRACT

Stacking fault energy (SFE) is one of the most important mechanical properties in structural material caused by the energy increment due to stacking sequence difference due to partial dislocations. Based on the analytic equation involving dislocation nucleation and stacking fault, new method of evaluating stacking fault energy by nanoindentation was suggested. Due to the limitation of the known analytic equation of dislocation nucleation energy considering only isotropy condition, some modifications were made.

In this study, the self-energy of dislocation and resolved shear stresses at dislocation nucleation were calculated with anisotropic material properties. For the elastic self-energy, known equation were used. For the resolved shear stresses at partial dislocation slip system, combination of nanoindentation experiment, electron backscatter diffraction (EBSD), and finite element (FE) simulation of nanoindentation were performed to obtain the dislocation nucleation strength. The results showed that the obtained dislocation nucleation shear stress was in the order of theoretical strength of dislocation nucleation and the stacking fault energy evaluated based on the results was on the range of known SFE values.

Keywords: Stacking fault energy (SFE), nanoindentation, dislocation

nucleation, dislocation energy barrier, anisotropy

Student number: 2014-21477

Contents

4. Methodology

5. Results and Discussion

LIST OF TABLES

LIST OF FIGURES

1. Introduction

Dislocation is an important type of defects that is essential for understanding mechanical properties of crystalline solids. In particular, yielding is thought to be mostly concerned with dislocation movements or nucleation by dislocation sources, etc. Since dislocation is of such importance, there have been numerous studies concerning the natures of dislocation, including its self-energy[1-6], strength of dislocation nucleation[7-10], energy barrier [10-16], and many others.

For face centered cubic (FCC) materials, dislocations are usually in the form of partial dislocations, which is caused by dissociation of perfect dislocation to lower the energy of dislocations. Due to the dissociation, the sequence of stacking is distorted to form the defect called stacking fault. The original stacking sequence of close packed plane in FCC crystal is ABCABCABC… However, if partial dislocations are generated, the stacking sequence changes to ABCACABC... , which is partly the stacking sequence of hexagonal closed packed (HCP) structure. Due to this defect, additional energy is generated (J/m2), or the force per unit length (N/m) is introduced as dissociated partial dislocations pull each other, which is the ‘stacking fault energy’ [7-9].

Stacking fault energy is one of the most important mechanical properties in structural materials that influence the deformation behavior[33]. It is known that stacking fault energy is closely related to materials' hardening behavior [7,9]. If stacking fault energy is high, the width between two dissociated partial dislocations are narrow, indicating the re-association of partial dislocations are easy, which allows the cross slip to occur easier, decreasing the hardening rate. For austenite, which is FCC phase steel, stacking fault energy is particularly important because deformation modes of austenite strongly depend on stacking fault energies [17-21]. If SFE is low, the main deformation mechanism becomes deformation induced martensitic transformation (DIMT), and if SFE is higher, the main deformation mode gradually changes to twin induced plasticity (TWIP) and if SFE is higher, the main mechanism of deformation is dislocation gliding [17]. Therefore, determining SFE is crucial in designing structural materials.

There are various methods of evaluating SFE, including transmission electron microscopy (TEM) observation[7,8], X-ray diffraction (XRD), or neutron diffraction[22]. However, sample preparation of TEM is difficult and the observation should be made several times to be the representative value. In addition, neutron diffraction is the most accurate way of calculating SFEs, but the

experiment is very time consuming. In addition to experimental measurements of SFE, first principle calculations were also done several times in order to estimate the generalized SFE[34-36], but there are some limits since numerical simulation considers the ideal case. In this study the new method of evaluating SFE is suggested by using the equation of dislocation nucleation energy and nanoindentation to nucleate the dislocation experimentally. Finite element calculation and electron backscatter diffraction (EBSD) analysis were performed in combination with nanoindentation experiment to modify the known equations of dislocation nucleation in isotropic medium, and consider anisotropy.

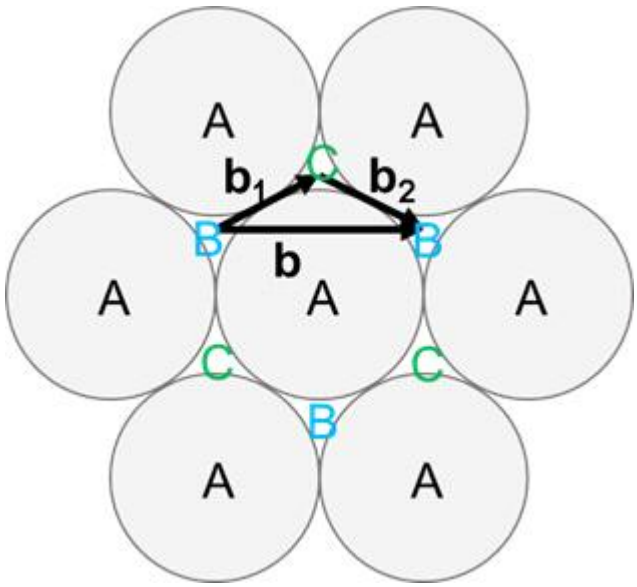

Figure 1.1 Burgers vector of perfect and partial dislocations in close packed plane of FCC structure. A, B, and C indicate atomic sites.

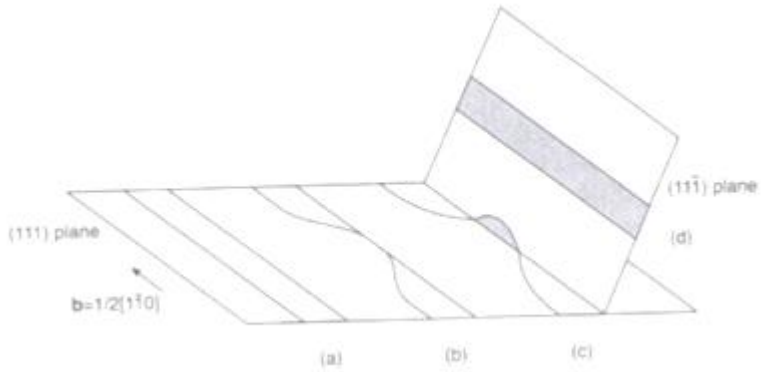

Figure 1.2 Cross slip of a dissociated dislocation (a) by formation of a constricted screw segment (b). The screw has dissociated on the cross-slip plane at (c) [7].

2. Theoretical Background

2.1. Dislocation nucleation energy in isotropic medium.

It is known that when performing a nanoindentation, dislocation loop is nucleated as plastic deformation initiates[23-32]. One of the simplest continuum models of energy of a dislocation loop consists of 3 terms: elastic energy of dislocation itself(E_{el}), stacking fault energy by partial dislocations(E_{SFE}), and the work done by shear stress(W_{ex}) when external force is applied(Eqn. 2.1)[10].

$$E = E_{el} + E_{SFE} - W_{ex} \qquad \text{(Equation 2.1)}$$

Since dislocation is a form of defect, energy increases by the elastic energy of dislocation itself. In FCC(Face Centered Cubic) material, dislocation usually nucleates in the form of partial dislocations, forming the region of stacking faults where stacking sequence is distorted, and as a result, additional energy is increased by this defect. The work done by shear stress(W_{ex}) when external force is applied lowers the energy of a dislocation.

Elastic self energy of a circular dislocation loop(E_{el}) in isotropic material has been developed over time[1-6]. One of the non-singular continuum models computed E_{el} when dislocation loop is circular and burgers vector of the dislocation loop is located in the

plane of the loop as

$$E_{el} = 2\pi R\frac{\mu b^2}{8\pi}[\frac{2-\nu}{1-\nu}(\ln\frac{8R}{\rho}-2)+\frac{1}{2}], \qquad \text{(Equation 2.2)}$$

where R is dislocation loop radius, μ, ν, b are material's shear modulus, Poisson's ratio, and size of the burgers vector, respectively[6]. ρ is the dislocation core radius or core cut off radius adopted for removal of singularity. Also, for prismatic dislocation loop where burgers vector is not located on the plane of the loop, E_{el} well approximated as[1,4,5]

$$E_{el} = \frac{\mu b^2 R}{2(1-\nu)}(\ln\frac{8R}{\rho}-1). \qquad \text{(Equation 2.3)}$$

The second term of right-hand side of the equation 2.1, E_{SFE} is the energy increment by development of stacking fault when partial dislocations are nucleated. For a circular dislocation, E_{SFE} can be expressed as

$$E_{SFE} = \gamma_{SFE}\pi R^2, \qquad \text{(Equation 2.4)}$$

where γ_{SFE} is the stacking fault energy of the material, and the term multiplied is the area of the stacking fault region developed.

The third therm of the right-hand side of the equation 2.1 (W_{ex}) is the work done by shear stress when external force is applied:

$$W_{ex} = b\tau\pi R^2, \qquad \text{(Equation 2.5)}$$

where τ is the shear stress developed by applied force.

In the work of Aubry et.al.[10], non-prismatic dislocation was considered and by analysing the equation 2.2 shear stress at dislocation nucleation, that is theoretical CRSS (Critical Resolved Shear Stress) was estimated by continuum model when μ, ν b, and γ_{SFE}. are known, and ρ was fitted to the atomistic simulation data. Table 2.1 shows the parameters used in this calculation. In order for the dislocation to nucleate energy barrier E_b should reach 0. E_b is simply the maximum of the equation 2.2, which is the maximum of E. E is the function of R and τ:

$$E(R,\tau) = 2\pi R\frac{\mu b^2}{8\pi}[\frac{2-\nu}{1-\nu}(\ln\frac{8R}{\rho}-2)+\frac{1}{2}]+\gamma_{SFE}\pi R^2-b\tau\pi R^2$$

(Equation 2.6)

The energy barrier is a function of τ:

$$E_b(\tau) = \max_{R>0}E(R,\tau). \qquad \text{(Equation 2.7)}$$

In figure 2.1(a), the E surface is plotted as a function of R and τ. When τ is fixed, E is plotted as a function of R, with maximum value(Fig. 2.1(b)). Therefore maximum value of E, which is the energy barrier E_b, can be obtained as a function of τ by partial differentiation of E with respect to R is 0(eqn.2.8).

$$\frac{\partial E}{\partial R} = \frac{\mu b^2}{4}[\frac{2-\nu}{1-\nu}(\ln\frac{8R}{\rho}-1)+\frac{1}{2}]+2\gamma_{SFE}\pi R-2b\tau\pi R=0 \quad \text{(Equation 2.8)}$$

With equation 2.8, R can be thought as a function of $\tau, R(\tau)$, although

it cannot be expressed easily. Therefore, E_b can be expressed with τ by

$$E_b(\tau) = 2\pi R(\tau)\frac{\mu b^2}{8\pi}[\frac{2-\nu}{1-\nu}(\ln\frac{8R(\tau)}{\rho}-2)+\frac{1}{2}]+\gamma_{SFE}\pi R(\tau)^2-b\tau\pi R(\tau)^2,$$

(Equation 2.9)

and when the energy barrier reaches 0, the dislocation loop is nucleated with certain τ,which is the dislocation nucleation strength, or CRSS, and its corresponding R(Fig. 2.2). R at dislocation nucleation can be thought as R_C, critical dislocation loop radius, when increment of R causes decrease in energy of dislocation, enabling the dislocation loop to expand after nucleation as can be seen in figure 2.1(b).

Table 2.1 parameters used for energy surface plot

G	44.6 GPa
v	0.41 GPa
γ_{SFE}	44.7mJ/m2
b	0.1468nm
ρ	1b

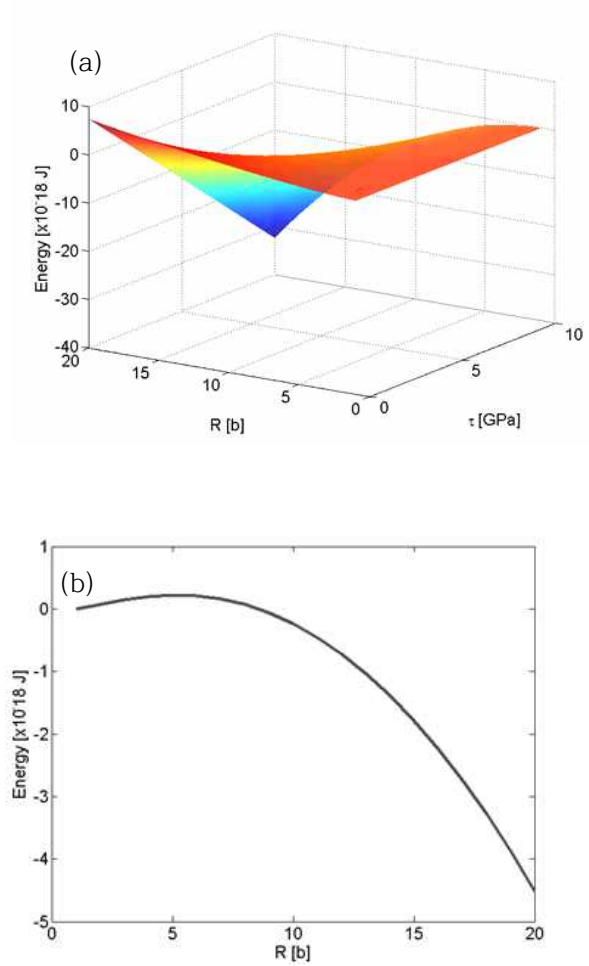

Figure 2.1 (a)Surface plot of energy of dislocation(E) as a function of dislocation loop radius(R) and applied shear stress(τ) and (b) E as a function of R with fixed τ.

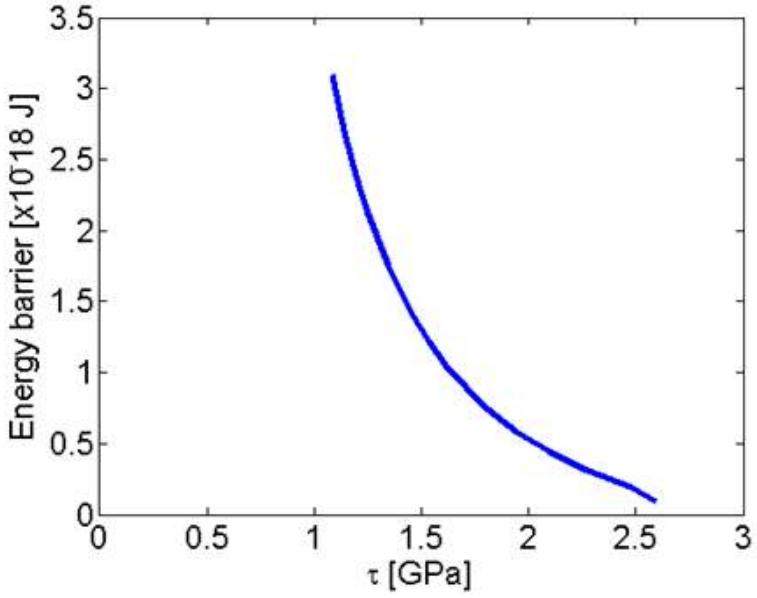

Figure 2.2 Energy barrier plotted as a function of τ

2.2. Maximum shear stress at dislocation nucleation in isotropic medium during nanoindentation

During the load controlled nanoindentation, load is applied to the specimen as the given load function, and the displacement caused by the pressure is recorded. As, a result, a load-displacement curve(LD curve) is obtained by nanoindentation. Figure 2.3 show the typical load-displacement curve during nanoindentaion. In the early stage of deformation, where only elastic deformation is present, experimental LD curve follows the well known Hertzian elastic contact solution [36], which is

$$P = \frac{4}{3} E_r \sqrt{R_{tip} h^3}, \qquad \text{(Equation 2.10)}$$

where P, E_r, R_{tip}, and h are applied force, reduced modulus, indenter tip radius, and penetration depth, respectively. Reduced modulus can be obtained if the elastic modulus and Poisson's ratio are known for the tip and the specimen as in equation 2.10, assuming isotropic condition

$$\frac{1}{E_r} = \frac{1-\nu_s^2}{E_s} + \frac{1-\nu_t^2}{E_t}. \qquad \text{(Equation 2.11)}$$

E_s, ν_s, E_t, and ν_t are elastic modulus of the specimen, Poisson's ratio of the specimen, elastic modulus of the indenter tip, and Poisson's ratio of the indenter tip, respectively[36].

As the load applied reaches certain value, there is a sudden

burst of displacement without load increasing, which is known as ‘pop-in’ behavior. Many studies have found out that this discontinuity of displacement is a sign of incipient plasticity[23-32], where the LD curve starts to deviate from elastic contact solution. For nanoindentation, it is thought that the initiation of plasticity is caused by nucleation of dislocation rather than moving the dislocation already existing in the specimen because the tip is small enough to regard the specimen as dislocation free. (However, since nanoindentation is sensitive to the surface condition and there are some probability that the indentation might be done near the pre-existing dislocation, the experiment is done for number of times and the results are analysed with cumulative probability.) Thus, maximum shear stress at pop-in load indicates the shear stress needed to nucleate a dislocation.

The stresses at specific load directly below the indenter tip was calculated by earlier studies[36]. If the tip is spherical, the stress fields will be axis symmetrical along the loading axis, z. Therefore, cylindrical coordinate system will be convenient for calculation. If r axis corresponds to radial direction and θ to tangential direction, the principal stresses can be expresses as

$$\sigma_r = \sigma_\theta = -p_0(1+\nu)[1-(z/a)\tan^{-1}(a/z)] + \frac{1}{2}p_0(1+z^2/a^2)^{-1},$$

(Equation 2.12)

$$\sigma_z = -p_0(1+z^2/a^2)^{-1}, \qquad \text{(Equation 2.13)}$$

where a is the contact area of indenter tip and the specimen and p_0 is the maximum pressure computed as

$$p_0 = (\frac{6PE_r^2}{\pi^3 R^2})^{1/3}. \qquad \text{(Equation 2.14)}$$

Maximum shear stress is the half of the difference between the maximum and the minimum principal stresses, which is approximately 31 percent of the maximum pressure, regarding ν_s as 0.3[36]:

$$\tau_m = \frac{1}{2}|\sigma_z - \sigma_r| \approx 0.31(\frac{6PE_r^2}{\pi^3 R^2})^{1/3}. \qquad \text{(Equation 2.15)}$$

Figure 2.4 is the stresses normalized by maximum pressure along the depth below the center of the indenter tip. From the plot, it can be noted that the maximum shear stress is not located in the surface of the specimen where the indenter tip is contacted, but somewhat below.

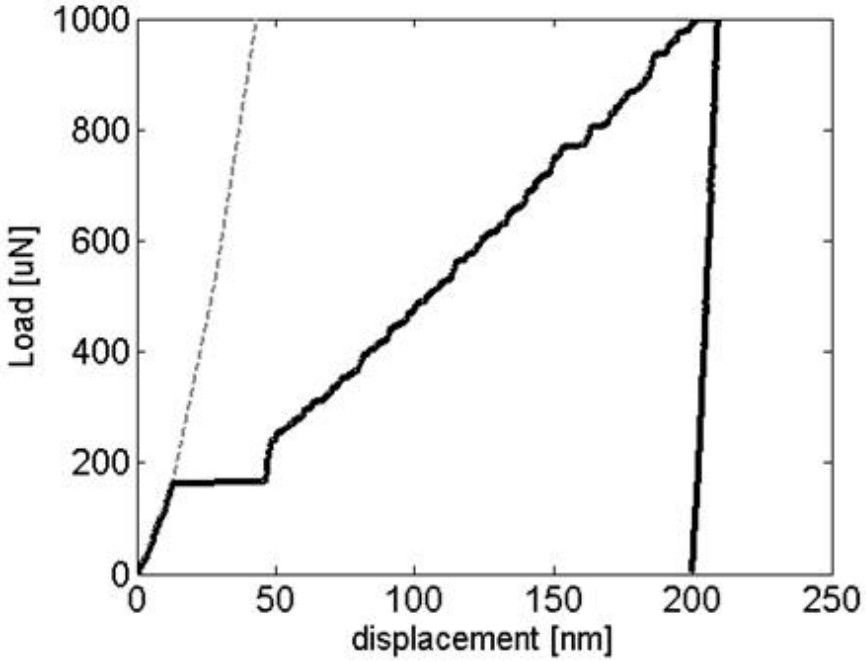

Figure 2.3 Load-displacement curve of a nanoindentaion(solid line) and Hertzian contact solution in dashed line.

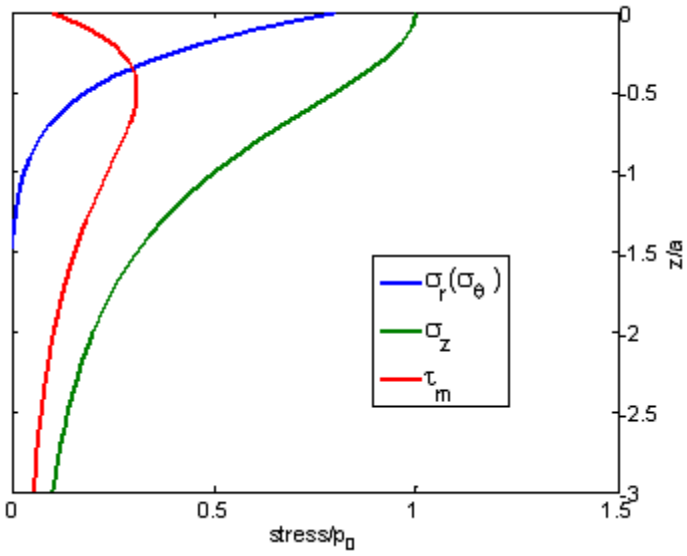

Figure 2.4 stress vs depth at r=a(contact radius) during indentation with spherical tip.

2.3. Evaluation of stacking fault energy.

As mentioned in section 2.3, maximum shear stress at dislocation nucleation in isotropic condition can be obtained from nanoindentation experiment. Then, by using the equation 2.6, the energy of circular dislocation loop γ_{SFE} can be estimated using similar operation done by Aubry et.al., when other parameters including μ, b, etc. except γ_{SFE} are known. The energy of dislocation loop can be plotted as a function of dislocation loop radius and stacking fault energy, and when partial derivative of dislocation energy with respect to dislocation loop radius is 0 and dislocation loop energy is also 0, the stacking fault energy value can be obtained(Fig. 2.6)

However, Since nanoindentation is conducted in single crystal level, isotropic assumption can have some error in it. For the elastic energy of a dislocation loop, the value may vary according to burgers vector direction, and the plane where the dislocation is located, and anisotropic, cubic materials have 3 independent elastic constants, C_{11}, C_{12}, and C_{44} rather than μ and ν. Therefore, more precise calculation must be done to calculate the elastic energy of a circular dislocation loop in anisotropic medium.

The shear stress for dislocation nucleation during nanoindentation should also be considered with anisotropy condition.

First of all, the experiment is done on grains with specific orientation, therefore, the responding load-displacement behavior varies accordingly. In addition, in crystal, dislocation is nucleated in certain slip systems, that is, {1 1 1}<1 1 0> systems in FCC materials and {1 1 0}<1 1 1> or {1 2 3}<1 1 0> slip systems in BCC materials[7-9]. The maximum value of the shear stress may not be on the slip system capable of dislocation nucleation, so the resolved shear stress on the specific slip system should be regarded for accuracy. Thus, the stress should be resolved to all the slip systems and the maximum values among those results should be the accurate CRSS with that specific slip system activating. With considering anisotropy, more precise estimation of stacking fault energy may be possible with nanoindentation experiment.

3. Experimental Procedure

3.1 Sample Preparation

The material used in this experiment is 99.99% pure Cu. Before performing nanoindentation, initial condition of the specimen was observed by electron backscatter diffraction(EBSD), TSL attached to scanning electron microscopy(SEM), SU70, Hitachi. Software OIM, TSL was used for the data analysis. Standard metallographic grinding and polishing procedure were done to remove the damaged layer. The polishing was finished with 0.1μm diamond suspension followed by electropolishing with D2 solution with chemical composition shown on table 3.1.

Spread was shown on EBSD mapping of Cu specimen(Fig.3.1) without any heat treatment, which indicates that there are defects such as dislocations exist in the specimen. To reduce the number of defects , heat treatment was conducted as following order. The specimen was heated to 500°C with heating rate of 50°C/min and held for 20minutes followed by water quenching. After the heat treatment, specimen were polished again, with the same procedure stated above. EBSD mapping of the specimen after the heat treatment shows that the sample did not show any spreading(figure 3.1) and this indicates that dislocation

density were reduced enough to regard it as fully annealed. With this annealed Cu specimen, the nanoindentaion was conducted.

Table 3.1 Chemical contents of D2 solution form electropolishing

	Phosphoric acid	Ethanol	n-Propylalcohol	Water
vol.%	25	20	5	bal.

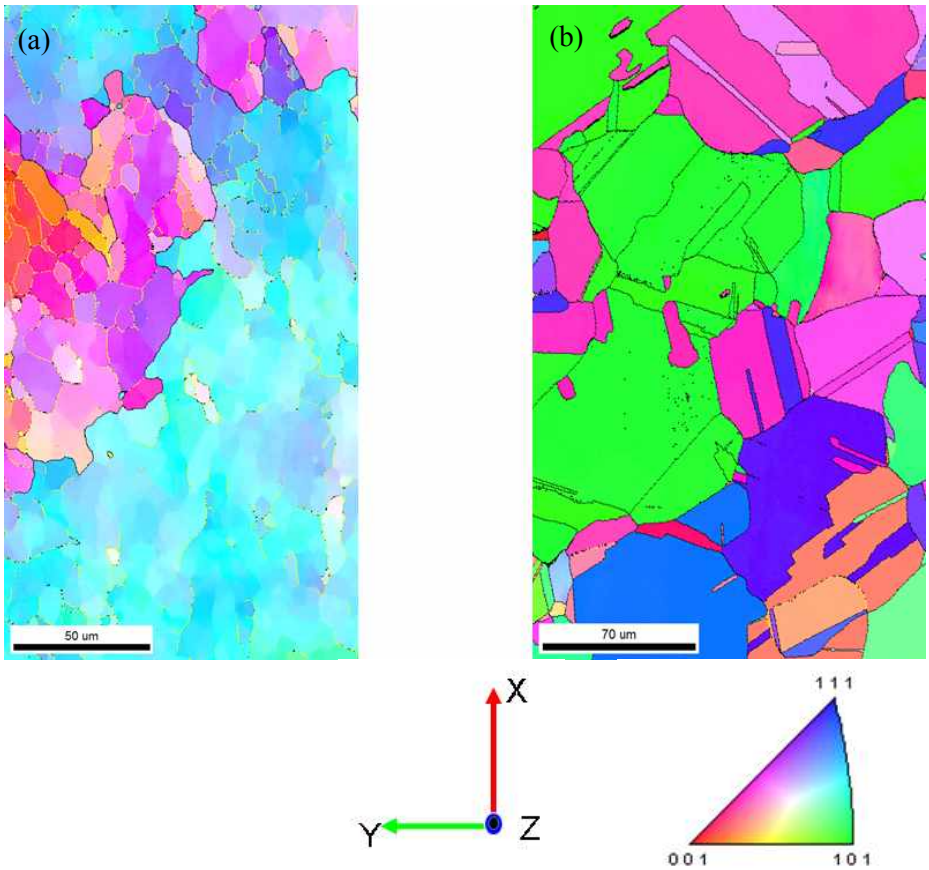

Figure 3.1 EBSD Z directional inverse pole figure map of Cu (a) without heat treatment and (b) after heat treatment.

3.2 Nanoindentation

Nanoindentation was conducted by TriboLab® 750 Ubi, Hystron equipped with diamond cono-spherical tip. Before experimenting on Cu specimen, nanoindentation on standard specimen were done to calculate the exact radius of the tip.

Tip radius of the tip used in this experiment was obtained by calculating the area function based on the indentation results conducted on standard fused quartz (FQ) sample. Equation 3.1 show the two-parameter relationship between contact depth hc and area A. Approximately this relationship can be reduced to equation 3.2. In this experiment, C0 and C1 obtained were −3.14 and 3276.50, respectively, thus R results in 580nm. [37-39] Also, it was verified by fitting the elastic region of the load-displacement curve to well-known Hertzian solution(Eqn. 3.3).

$$A = C_0 h_c^2 + C_1 h_c \qquad \text{(Equation 3.1)}$$

$$C_1 = 2\pi R \qquad \text{(Equation 3.2)}$$

$$P = \frac{4}{3} E_r R^{\frac{1}{2}} h^{\frac{3}{2}} \qquad \text{(Equation 3.3)}$$

(P: Load, Er: reduced modulus, R: tip radius, h: depth)

Nanoindentation was performed in 14x14 grid and in 20x20 grid, total of 596 indents, to obtain enough experimental data on

various grain orientations. The spacings between each of the indent were set as 10μm to avoid any influence by indentation marks. Load controlled indentation was performed with peak load of 2000μN and loading, holding, unloading time was set as 5seconds, 2seconds, 5seconds, respectively.

(a)

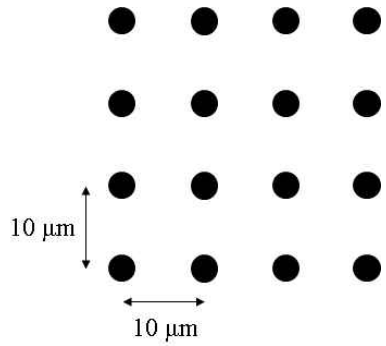

(b)

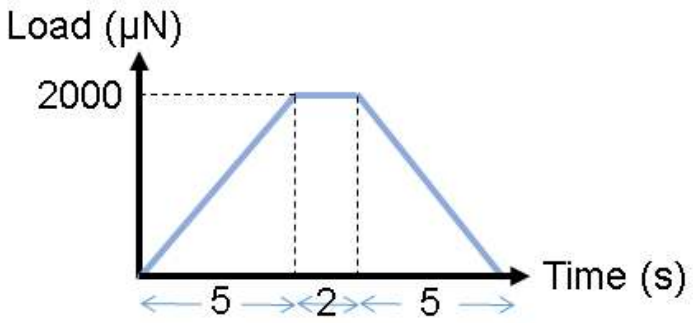

Figure 3.3 (a) Nanoindentation grid and (b) loading rate

3.3 Electron Backscatter Diffraction Analysis

Electron backscatter diffraction (EBSD) analysis was conducted for Cu specimen before and after the heat treatment in order to confirm that the specimen can be regarded as fully annealed. As mentioned above, EBSD mapping before heat treatment showed spreading (Fig.3.1.) while heat treated specimen does not show any spreading.

EBSD analysis was also conducted after the nanoindentation experiment to identify crystallographic orientation of each indented grain. Confidence index below 0.1 were deleted from the data.

4. Methodology

4.1 Elastic Energy of Dislocation Loop in Anisotropic Medium

Calculation of elastic energy of a dislocation loop involves concept of eigenstrain. “Eigenstrain”, which means nonelastic strains such as thermal expansion, phase transformation, plastic strain, and misfit strain, ets. In the case of dislocations, eigenstrains originate from burgers vector **b** by relative slip of a plane containing a dislocation[2].

Total strain ϵ_{ij} can be regarded as sum of elastic straine_{ij} and eigenstrain$\epsilon^*{}_{ij}$(Eqn.4.1), and total strain is compatible(Eqn.4.2).

$$\epsilon_{ij} = e_{ij} + \epsilon^*{}_{ij} \qquad \text{(Equation 4.1)}$$

$$\epsilon_{ij} = \frac{1}{2}(u_{i,j} + u_{j,i}) \qquad \text{(Equation 4.2)}$$

where, $u_{i,j} = \partial u_i / \partial x_j$.

Elastic stress σ_{ij}can be obtained by Hooke’s law;

$$\sigma_{ij} = C_{ijkl} e_{kl} = C_{ijkl}(\epsilon_{kl} - \epsilon^*{}_{kl}) = C_{ijkl}(u_{k,l} - \epsilon^*{}_{kl}) \qquad \text{(Equation 4.3)}$$

where C_{ijkl} are the elastic constants[2].

Elastic self energy of a circular dislocation loop originates from eigenstress caused by eigenstrain due to singularity along the dislocation line. And when calculating eigenstresses, any external force or surface constraint are assumed to be non-existing along the material domain.

With these conditions taken into account, equations of equilibrium(Eqn.5.4) and boundary conditions(Eqn.4.5) are as follows:

$$\sigma_{ij,j} = 0 \quad (i = 1,2,3) \qquad \text{(Equation 4.4)}$$

$$\sigma_{ij} n_j = 0 \qquad \text{(Equation 4.5)}$$

where n_i is the exterior unit normal vector on the boundary of material domain.

Substitution of equation 4.3 into equations 4.4 and 4.5 results in following equations 4.6 and 4.7.

$$C_{ijkl} u_{k,lj} = C_{ijkl} \epsilon^*{}_{kl,j} \qquad \text{(Equation 4.6)}$$

$$C_{ijkl} u_{k,l} n_j = C_{ijkl} \epsilon^*{}_{kl} n_j \qquad \text{(Equation 4.7)}$$

Equation 4.6 is the fundamental equation to be solved. When $\epsilon^*{}_{ij}(\boldsymbol{x})$ is expressed in the form of a single wave with amplitude $\bar{\epsilon}^*{}_{ij}(\boldsymbol{\xi})$ and the wave vector $\boldsymbol{\xi}$, it can be written as in equation 4.8:

$$\epsilon^*{}_{ij}(\boldsymbol{x}) = \bar{\epsilon}^*{}_{ij}(\boldsymbol{\xi}) \exp(i\boldsymbol{\xi} \cdot \boldsymbol{x}). \qquad \text{(Equation 4.8)}$$

($i = \sqrt{-1}$ and $\boldsymbol{\xi} \cdot \boldsymbol{x} = \xi_k x_k$)

The solution of equation 4.6 ,$u_i(\boldsymbol{x})$, is also in the form of a single wave with same wave vector $\boldsymbol{\xi}$, as expressed in equation 4.9 below:

$$u_i(\boldsymbol{x}) = \bar{u}_i(\boldsymbol{\xi}) \exp(i\boldsymbol{\xi} \cdot \boldsymbol{x}). \qquad \text{(Equation 4.9)}$$

Substitution of equations 4.8 and 4.9 into equation 4.6 results in

$$C_{ijkl} \overline{u_k} \xi_l \xi_j = -i C_{ijkl} \bar{\epsilon}^*{}_{kl} \xi_j \qquad \text{(Equation 4.10)}$$

$$(i = 1,2,3)$$

The notations $K_{ik}(\boldsymbol{\xi}), X_i$ are introduced(eqn. 4.10) to change the form of equation 4.10 into

$$K_{ik}(\boldsymbol{\xi}) = C_{ijkl}\xi_j\xi_{l,} \qquad \text{(Equation 4.11)}$$
$$X_i = -iC_{ijkl}\bar{\epsilon}^*{}_{kl}\xi_j$$

$$K_{ij}\overline{u_j} = X_i \quad (i = 1,2,3). \qquad \text{(Equation 4.12)}$$

$\overline{u_i}(\boldsymbol{\xi})$ can be obtained by following operation,

$$\overline{u_i}(\boldsymbol{\xi}) = X_j N_{ij}(\boldsymbol{\xi})/D(\boldsymbol{\xi}) \qquad \text{(Equation 4.13)}$$

where $D(\boldsymbol{\xi})$ and $N_{ij}(\boldsymbol{\xi})$ are determinant and cofactors of matrix $\boldsymbol{K}(\boldsymbol{\xi})$. Substituting equation 4.13 into 4.9 results in:

$$u_i(\boldsymbol{x}) = -iC_{jlmn}\bar{\epsilon}^*{}_{mn}(\boldsymbol{\xi})\xi_l N_{ij}(\boldsymbol{\xi})D^{-1}(\boldsymbol{\xi})\exp(i\boldsymbol{\xi}\cdot\boldsymbol{x}) \qquad \text{(Equation 4.14)}$$

Corresponding strain(eqn.4.15) and stress(eqn.4.16) are obtained by simple derivation.

$$\epsilon_{ij}(\boldsymbol{x}) = \frac{1}{2}C_{klmn}\bar{\epsilon}^*{}_{mn}(\boldsymbol{\xi})\xi_l[\xi_j N_{ik}(\boldsymbol{\xi}) + \xi_i N_{jk}(\boldsymbol{\xi})]D^{-1}(\boldsymbol{\xi})\exp(i\boldsymbol{\xi}\cdot\boldsymbol{x})$$

(Equation 4.15)

$$\sigma_{ij}(\boldsymbol{x}) = C_{ijkl}[C_{pqmn}\bar{\epsilon}^*{}_{mn}(\boldsymbol{\xi})\xi_q\xi_l N_{kp}(\boldsymbol{\xi})D^{-1}(\boldsymbol{\xi})\exp(i\boldsymbol{\xi}\cdot\boldsymbol{x}) - \epsilon^*{}_{kl}(\boldsymbol{x})]$$

(Equation 4.16)

In linear theory of elasticity, the superposition of solutions are allowed, which enables us to utilize Fourier integrals. If $\epsilon^*{}_{ij}(\boldsymbol{x})$ is expressed in Fourier integral form,

$$\epsilon^*_{ij}(\boldsymbol{x}) = \int_{-\infty}^{\infty} \bar{\epsilon}^*_{ij}(\boldsymbol{\xi})\exp(i\boldsymbol{\xi}\cdot\boldsymbol{x})d\boldsymbol{\xi} \qquad \text{(Equation 4.17)}$$

where

$$\bar{\epsilon}^*_{ij}(\boldsymbol{\xi}) = (2\pi)^{-3}\int_{-\infty}^{\infty} \epsilon^*_{ij}(\boldsymbol{x})\exp(-i\boldsymbol{\xi}\cdot\boldsymbol{x})d\boldsymbol{x} \qquad \text{(Equation 4.18)}$$

and

$$u_i(\boldsymbol{x}) = -i\int_{-\infty}^{\infty} C_{jlmn}\bar{\epsilon}^*_{mn}(\boldsymbol{\xi})\xi_l N_{ij}(\boldsymbol{\xi})D^{-1}(\boldsymbol{\xi})\exp(i\boldsymbol{\xi}\cdot\boldsymbol{x})d\boldsymbol{\xi}$$

(Equation 4.19)

The final expressions of the solution is,

$$u_i(\boldsymbol{x}) = -i(2\pi)^{-3}\int_{-\infty}^{\infty}\int_{-\infty}^{\infty} C_{jlmn}\epsilon^*_{mn}(\boldsymbol{x}')\xi_l N_{ij}(\boldsymbol{\xi})D^{-1}(\boldsymbol{\xi}) \qquad \text{(Equation 4.20)}$$
$$\times \exp(i\boldsymbol{\xi}\cdot(\boldsymbol{x}-\boldsymbol{x}'))d\boldsymbol{\xi}d\boldsymbol{x}'$$

$$\epsilon_{ij}(\boldsymbol{x}) = (2\pi)^{-3}\int_{-\infty}^{\infty}\int_{-\infty}^{\infty}\frac{1}{2}C_{klmn}\epsilon^*_{mn}(\boldsymbol{x}') \qquad \text{(Equation 4.21)}$$
$$\times\xi_l[\xi_j N_{ik}(\boldsymbol{\xi}) + \xi_i N_{jk}(\boldsymbol{\xi})]D^{-1}(\boldsymbol{\xi})$$
$$\times \exp[i\boldsymbol{\xi}\cdot(\boldsymbol{x}-\boldsymbol{x}')]d\boldsymbol{\xi}d\boldsymbol{x}'$$

$$\sigma_{ij}(\boldsymbol{x}) = C_{ijkl}[(2\pi)^{-3}\int_{-\infty}^{\infty}\int_{-\infty}^{\infty}\frac{1}{2}C_{pqmn}\epsilon^*_{mn}(\boldsymbol{x}')\xi_q\xi_l N_{kp}(\boldsymbol{\xi})D^{-1}(\boldsymbol{\xi})$$
$$\times \exp[i\boldsymbol{\xi}\cdot(\boldsymbol{x}-\boldsymbol{x}')]d\boldsymbol{\xi}d\boldsymbol{x}' - \epsilon^*_{kl}(\boldsymbol{x})] \qquad \text{(Equation 4.21)}$$

Displacement gradient $u_{i,j}$ consists of elastic distortion β_{ji} and plastic distortion β^*_{ji} according to Kroner(1958). Thus, the total strain,

elastic strain and eigenstrain defined above(eqn. 4.1 and 4.2) can be expressed as

$$\epsilon_{ij} = \frac{1}{2}(u_{i,j} + u_{j,i}), \qquad \text{(Equation 4.22)}$$

$$e_{ij} = \frac{1}{2}(\beta_{ij} + \beta_{ji}), \qquad \text{(Equation 4.23)}$$

$$\epsilon^*{}_{ij} = \frac{1}{2}(\beta^*{}_{ij} + \beta^*{}_{ji}), \qquad \text{(Equation 4.24)}$$

respectively.

For the case of dislocation, particularly dislocation loop, $\beta^*{}_{ji}(\boldsymbol{x})$ is caused by slip $b_i$of the plane S with its normal vector n_j and can be expressed as following:

$$\beta^*{}_{ji}(\boldsymbol{x}) = -\, b_i n_j \delta(\boldsymbol{S} - \boldsymbol{x}) \qquad \text{(Equation 4.25)}$$

$$\epsilon^*{}_{ij}(\boldsymbol{x}) = -\,\frac{1}{2}(b_i n_j + b_j n_i)\delta(\boldsymbol{S} - \boldsymbol{x}) \qquad \text{(Equation 4.26)}$$

When Green's function $G_{ij}(\boldsymbol{x} - \boldsymbol{x}')$ is defined as

$$G_{ij}(\boldsymbol{x} - \boldsymbol{x}') = (2\pi)^{-3} \int_{-\infty}^{\infty} N_{ij}(\boldsymbol{\xi}) D^{-1}(\boldsymbol{\xi}) \exp[i\boldsymbol{\xi} \cdot (\boldsymbol{x} - \boldsymbol{x}')] d\boldsymbol{\xi}, \qquad \text{(Equation 4.27)}$$

u_i can be expressed as

$$u_i(\boldsymbol{x}) = \int_{\boldsymbol{S}} C_{jlmn} b_m G_{ij,l}(\boldsymbol{x} - \boldsymbol{x}') n_n dS(\boldsymbol{x}'), \qquad \text{(Equation 4.28)}$$

where $\boldsymbol{S}$ is the surface that the dislocation exists.

By differentiation of equation 4.28, total distortion and elastic

distortion can be obtained(eqn. 4.29 and eqn. 4.30)

$$u_{i,j}(\boldsymbol{x}) = \int_{\boldsymbol{S}} C_{klmn} b_m G_{ik,lj}(\boldsymbol{x}-\boldsymbol{x}') n_n dS(\boldsymbol{x}'), \quad \text{(Equation 4.29)}$$

$$\beta_{ji}(\boldsymbol{x}) = \int_{\boldsymbol{S}} C_{klmn} b_m G_{ik,lj}(\boldsymbol{x}-\boldsymbol{x}') n_n dS(\boldsymbol{x}') + b_i n_j \delta(\boldsymbol{S}-\boldsymbol{x}).$$

(Equation 4.30)

The Mura formula(1963) is obtained as in equation 4.31 by integration of equation 4.30 using Stokes' theorem,

$$\beta_{ji}(\boldsymbol{x}) = \int_{\boldsymbol{L}} \epsilon_{jnh} C_{pqmn} G_{ip,q}(\boldsymbol{x}-\boldsymbol{x}') b_m v_h dl(\boldsymbol{x}') \quad \text{(Equation 4.31)}$$

where ϵ_{ijk} is the permutation tensor, $\boldsymbol{v}$ is the direction of the dislocation line, and $\boldsymbol{L}$ is the boundary of the surface that the dislocation exist. Stress components are

$$\sigma_{ij}(\boldsymbol{x}) = C_{ijkl} \int_{\boldsymbol{L}} \epsilon_{lnh} C_{pqmn} G_{kp,q}(\boldsymbol{x}-\boldsymbol{x}') b_m v_h dl(\boldsymbol{x}'). \quad \text{(Equation 4.32)}$$

The Fourier integral expression for equation 4.31 are

$$\beta_{ji}(\boldsymbol{x}) = -i(2\pi)^{-3} \int_{\boldsymbol{L}} v_h dl(\boldsymbol{x}') \int_{-\infty}^{\infty} \epsilon_{jnh} C_{pqmn} \xi_q N_{ip}(\boldsymbol{\xi}) D^{-1}(\boldsymbol{\xi}) b_m \times \exp[i\boldsymbol{\xi} \cdot (\boldsymbol{x}-\boldsymbol{x}')] d\boldsymbol{\xi} \quad \text{(Equation 4.33)}$$

,

or

$$\beta_{ji}(\boldsymbol{x}) = -i(2\pi)^{-3} \int_{\boldsymbol{L}} dx'_h \int_{-\infty}^{\infty} \epsilon_{jnh} C_{pqmn} \xi_q N_{ip}(\boldsymbol{\xi}) D^{-1}(\boldsymbol{\xi}) b_m \times \exp[i\boldsymbol{\xi} \cdot (\boldsymbol{x}-\boldsymbol{x}')] d\boldsymbol{\xi}. \quad \text{(Equation 4.34)}$$

Distortion of a dislocation loop can be obtained from summation of a finite number of dislocation segments. Figure 4.1 shows the dislocation segment yz. An arbitrary point x' on the segment can be expressed as

$$\boldsymbol{x'} = \boldsymbol{y} + l(\boldsymbol{z}-\boldsymbol{y}),\ 0 \le l \le 1, \qquad \text{(Equation 4.35)}$$
$$dx_h = (z_h - y_h)dl,$$

and $\boldsymbol{\xi}$-space volume element is given by, $\boldsymbol{\xi} = \xi^2 d\xi d\boldsymbol{S}(\bar{\boldsymbol{\xi}})$, where $d\boldsymbol{S}(\bar{\boldsymbol{\xi}})$ is the $\boldsymbol{\xi}$-space surface element of the unit sphere S^2 and $\bar{\boldsymbol{\xi}} = \boldsymbol{\xi}/\xi$ and $\xi = |\boldsymbol{\xi}|$. Willis has integrated equation 4.34, obtaining

$$\beta_{ji} = \frac{-i}{(2\pi)^3}\epsilon_{jnh} C_{klmn} b_m (z_h - y_h) \int_{S^2} \frac{\bar{\xi}_l N_{ik}(\bar{\boldsymbol{\xi}}) d\boldsymbol{S}(\bar{\boldsymbol{\xi}})}{D(\bar{\boldsymbol{\xi}})[\bar{\boldsymbol{\xi}} \cdot (\boldsymbol{y}-\boldsymbol{x})][\bar{\boldsymbol{\xi}} \cdot \boldsymbol{z}-\boldsymbol{x})]}$$

(Equation 4.36)

Unit vectors $\boldsymbol{n}$, $\boldsymbol{m}^*$, and $\boldsymbol{m}$, which are plane normal, orthogonal to $\boldsymbol{y}-\boldsymbol{x}$ and $\boldsymbol{n}$, and orthogonal to $\boldsymbol{z}-\boldsymbol{x}$ and $\boldsymbol{n}$, respectively, as shown in figure 4.1 are introduced to express $\bar{\boldsymbol{\xi}}$ as

$$\bar{\boldsymbol{\xi}} = -\boldsymbol{m}^* \sin\phi + \boldsymbol{n}\cos\phi + h(\boldsymbol{y}-\boldsymbol{x})/|\boldsymbol{y}-\boldsymbol{x}|,\ |h| \le \epsilon \ll 1$$

(Equation 4.37)

with adoption of parameters ϕ and h, where h is infinitesimally small. Then the integral on equation 4.36 on S^2 becomes

$$\int_{S^2} = -\int_0^{2\pi} d\phi \int_{-\epsilon}^{\epsilon} dh \frac{(-m_{*_l}\sin\phi + n_l\cos\phi) N_{ik}(-\boldsymbol{m}^*\sin\phi + \boldsymbol{n}\cos\phi)}{D(-\boldsymbol{m}^*\sin\phi + \boldsymbol{n}\cos\phi)\sin\phi[\boldsymbol{m}^* \cdot (\boldsymbol{z}-\boldsymbol{y})]h|\boldsymbol{y}-\boldsymbol{x}|}$$

(Equation 4.38)

From figure 4.1, equation 4.38 can be derived.

$$[\boldsymbol{m}^* \cdot (\boldsymbol{z}-\boldsymbol{y})]|\boldsymbol{y}-\boldsymbol{x}| = r|\boldsymbol{z}-\boldsymbol{y}| = 2\times\text{area of triangle } xyz$$

$$(z_h - y_h)/|\boldsymbol{z}-\boldsymbol{y}| = v_h \qquad \text{(Equation 4.39)}$$

Also,

$$\int_{-\epsilon}^{\epsilon} \frac{dh}{h} = i\pi,$$

where r is the distance between $\boldsymbol{x}$ and dislocation line yz.

By similar calculation along $\boldsymbol{S^2}$ for $\boldsymbol{m}$ instead of $\boldsymbol{m}^*$, equation 4.36 becomes

$$\beta_{ji} = \frac{1}{(2\pi)^3}\epsilon_{jnh}C_{klmn}b_m v_h r^{-1}\times[\frac{1}{2}\int_0^{2\pi}[\frac{m^*{}_l N_{ik}(-\boldsymbol{m}^*\sin\phi+\boldsymbol{n}\cos\phi)}{D(-\boldsymbol{m}^*\sin\phi+\boldsymbol{n}\cos\phi)}$$

$$-\frac{\cos\phi}{\sin\phi}n_l[\frac{N_{ik}(-\boldsymbol{m}^*\sin\phi+\boldsymbol{n}\cos\phi)}{D(-\boldsymbol{m}^*\sin\phi+\boldsymbol{n}\cos\phi)}-\frac{N_{ik}(\boldsymbol{n})}{D(\boldsymbol{n})}]]d\phi$$

$$-\frac{1}{2}\int_0^{2\pi}[\frac{m^*{}_l N_{ik}(-\boldsymbol{m}sin\phi+\boldsymbol{n}\cos\phi)}{D(-\boldsymbol{m}sin\phi+\boldsymbol{n}\cos\phi)}$$

$$-\frac{\cos\phi}{\sin\phi}n_l[\frac{N_{ik}(-\boldsymbol{m}sin\phi+\boldsymbol{n}\cos\phi)}{D(-\boldsymbol{m}sin\phi+\boldsymbol{n}\cos\phi)}-\frac{N_{ik}(\boldsymbol{n})}{D(\boldsymbol{n})}]]d\phi] \qquad \text{(Equation 4.40)}$$

I_{lik} is introduced(eqn.4.41) to express the equation 4.40 to equation 4.42.

$$I_{lik}(\boldsymbol{m}^*,\boldsymbol{n}) = \int_0^{2\pi}[\frac{m^*{}_l N_{ik}(-\boldsymbol{m}^*\sin\phi+\boldsymbol{n}\cos\phi)}{D(-\boldsymbol{m}^*\sin\phi+\boldsymbol{n}\cos\phi)} \qquad \text{(Equation 4.41)}$$

$$- \frac{\cos\phi}{\sin\phi} n_l [\frac{N_{ik}(-\boldsymbol{m}^* \sin\phi + \boldsymbol{n}\cos\phi)}{D(-\boldsymbol{m}^* \sin\phi + \boldsymbol{n}\cos\phi)} - \frac{N_{ik}(\boldsymbol{n})}{D(\boldsymbol{n})}]] d\phi$$

$$\beta_{ji}(\boldsymbol{x}) = \frac{1}{(2\pi)^2} \epsilon_{jnh} C_{lkmn} b_m v_h r^{-1} [\frac{1}{2} I_{lik}(\boldsymbol{m}^*, \boldsymbol{n}) - \frac{1}{2} I_{lik}(\boldsymbol{m}, \boldsymbol{n})]$$

$$\equiv - v_h r^{-1} [\frac{1}{2} \Sigma_{jih}(\boldsymbol{m}^*, \boldsymbol{n}) - \frac{1}{2} \Sigma_{jih}(\boldsymbol{m}, \boldsymbol{n})] \qquad \text{(Equation. 4.42)}$$

For calculation of the distortion by a dislocation loop, integration of equation 4.42 along the dislocation line is done, which is

$$\beta_{ji}(\boldsymbol{x}) = - \frac{1}{8\pi^2} \epsilon_{jnh} C_{lkmn} b_m \oint_L v_h r^{-1} \frac{d}{dl} I_{lik}(\boldsymbol{m}, \boldsymbol{n}) dl \qquad \text{(Equation. 4.43)}$$

If the dislocation loop is a smooth curve, equation 4.43 can be written as equation 4.44 and with integration by parts, it can be written as equation 4.45.

$$\beta_{ji}(\boldsymbol{x}) = \frac{1}{8\pi^2} \epsilon_{jnh} C_{lkmn} b_m \oint_L \frac{d}{dl} (\frac{v_h}{r}) I_{lik}(\boldsymbol{m}, \boldsymbol{n}) dl \qquad \text{(Equation. 4.44)}$$

$$\beta_{ji}(\boldsymbol{x}) = - \frac{1}{2} \oint_L \frac{d}{dl} (\frac{v_h}{r}) \Sigma_{jih}(\boldsymbol{m}, \boldsymbol{n}) dl \qquad \text{(Equation. 4.45)}$$

Figure 4.2(a) shows the dislocation loop L and vectors describing it. Vector $\boldsymbol{t}$ and angle θ and α are introduced which is $\boldsymbol{x}' - \boldsymbol{x}$, angle between $\boldsymbol{t}$ and some datum, and angle between $\boldsymbol{v}$ and the datum, respectively, as shown in figure 4.2(b). Then, the follwing equations are obtained:

$$dl \sin(\theta - \alpha) = |\boldsymbol{x} - \boldsymbol{x}'| d\theta,$$

$$dl \cos(\theta - \alpha) = - d|\boldsymbol{x} - \boldsymbol{x}'|,$$

$$r = |\boldsymbol{x} - \boldsymbol{x}'| \sin(\theta - \alpha), \qquad \text{(Equation. 4.46)}$$

$$d\alpha = \kappa dl,$$

$$dv_h = \rho_h d\alpha,$$

where κ is the curvature of L at $\boldsymbol{x}'$, and ρ is the unit vector with direction towards the center of curvature. Then, the equation 4.45 is expressed as an integration over θ,

$$\beta_{ji}(\boldsymbol{x}) = \frac{1}{2} \oint_L \kappa \sum_{ji}(\theta) \csc^3(\theta - \alpha) d\theta, \qquad \text{(Equation. 4.46)}$$

where

$$\sum_{ji}(\theta) = t_h \sum_{jih}(\boldsymbol{m}, \boldsymbol{n}) \qquad \text{(Equation. 4.47)}$$

In current study, the dislocation loop is considered circular, that is, $\theta - \alpha = \frac{\pi}{2}$, with radius of r ($\kappa = 1/r$). Then, if the center of the dislocation loop is assumed to be at the origin O, position along the dislocation loop $\boldsymbol{x}'$ can be expressed as $\boldsymbol{x}' = (r\cos\theta', r\sin\theta', 0)$, with introduction of an angle θ', which is the angle between $O\boldsymbol{x}'$ and the datum.

Then, θ and α can be expressed as a function of θ' and the integration along the dislocation line L becomes integration over θ' from 0 to 2π. After calculating elastic distortion, elastic stress field can be obtained by

$$\sigma_{ij} = C_{ijkl}\beta_{kl} \qquad \text{(Equation. 4.48)}$$

and the elastic strain energy caused by a plastic distortion is

$$W^* = \frac{1}{2}\int_{\boldsymbol{D}} \sigma_{ij} e_{ij} d\boldsymbol{D}. \qquad \text{(Equation. 4.49)}$$

where D is the domain, or the sample size. Since elastic strain can be expressed with subtraction of total strain and eigenstrain.

$$W^* = \frac{1}{2}\int_{\boldsymbol{D}} \sigma_{ij}(\epsilon_{ij} - \epsilon^*{}_{ij}) d\boldsymbol{D} \qquad \text{(Equation 4.50)}$$

Total strain ϵ_{ij} can be expresses as $\frac{1}{2}(u_{i,j} - u_{j,i})$, and by integration by parts,

$$\int_D \sigma_{ij} u_{i,j} dD = \int_S \sigma_{ij} u_i n_j dS - \int_D \sigma_{ij,j} u_i dD, \qquad \text{(Equation 4.51)}$$

and with condition of free surface and equilibrium, the equation 4.51 becomes 0. Therefore, the elastic energy can be obtained with only plastic distortion, which is defined in the 2-D surface of S:

$$W^* = \frac{1}{2}\int_{\boldsymbol{S}} \sigma_{ij} b_i n_j d\boldsymbol{S} \qquad \text{(Equation 4.52)}$$

Position $\boldsymbol{x}$ was defined only inside the loop since all the integration were done inside the loop, which can be expressed with R and γ, which is the length of $O\boldsymbol{x}$ and the angle between $O\boldsymbol{x}$ and the datum:

$$\boldsymbol{x}' = (R\cos\gamma, R\sin\gamma, 0). \qquad \text{(Equation. 4.53)}$$

So the equation 4.49 can be expressed as

$$W^* = \frac{1}{2}\int_0^{2\pi}\int_0^r \sigma_{ij}(R,\gamma) b_i n_j R dR d\gamma. \qquad \text{(Equation. 4.54)}$$

In Chu's study, self energy of elliptical dislocation loops in anisotropic crystals were calculated by these numerical integration. Chu suggested that the dislocation self energy normalized by material constants can be expressed as following:

$$\frac{E_{self}}{\mu_e b^2 r_e} = A[\ln(\frac{r_e}{\rho}) - B'], \qquad \text{(Equation. 4.55)}$$

where μ_e is an equivalent shear modulus, $\frac{1}{3}(C_{11} - C_{12} + C_{44})$, defined in the (1 1 1) plane, closed packed plane, of FCC crystal [40]. r_e is the equivalent radius, which is $l_{loop}/2\pi$, l_{loop} being the length of the dislocation loop. ρ and b are core cut-off radius and burgers vector, respectively. Parameters A and B are dimensionless and independent of material properties and Chu fitted the parameters A and B by variation of dislocation shape, or the aspect ratio of ellipse, $\cos\theta$. The results showed that $A = 0.1119 - 0.01312\cos\theta$ and $B' = 2.371 + 1.622(1 - \cos\theta)^2$. With this equations, the elastic self energy of circular dislocation loops were evaluated with consideration of anisotropy.

Table 4.1 Elastic constants of Cu

	C_{11}	C_{12}	C_{44}
Cu	168.4 GPa	121.4 GPa	75.4 GPa

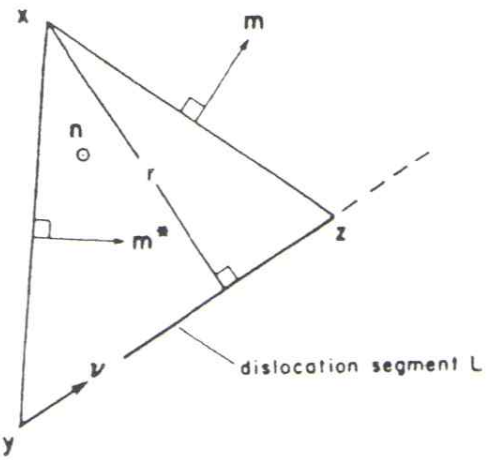

Figure4.1 Dislocation segment yz, with unit vector n normal to the plane xyz[2].

(a)

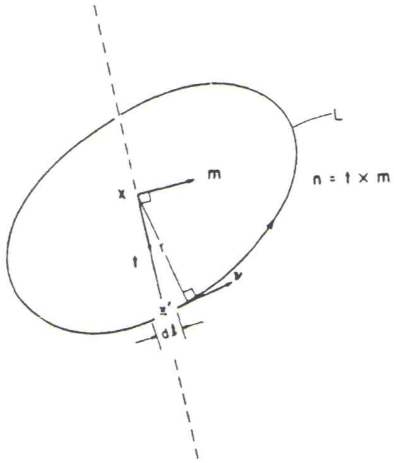

(b)

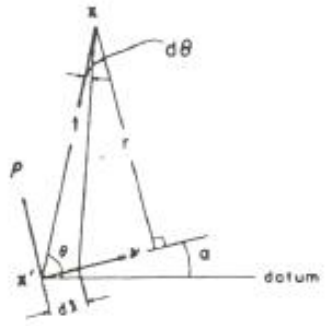

Figure 4.2 (a) Dislocation loop L and related vectors, and (b) Geometry at dislocation line element dl.

4.2 Finite Element Simulation of Nanoindentation and Calculation of Maximum Shear Stress at Dislocation Nucleation

FE(Finite Element) simulations of a nanoindentation on single grain with different orientations were performed using the commercial software ABAQUS (Ver.6.10) to determine the stress field σ_{ij} inside the grains.

The orientation data of the grains was obtained from EBSD analysis of the indented surface by nanoindentation experiments. Table 4.2 shows the grain numbers and their corresponding orientation data of the FE simulation performed. Only elastic deformation was considered and the elastic constants of pure Cu were used, shown in table 4.1. The indenter tip was regarded as spherical rigid body, with tip radius of 580nm which is obtained from the actual tip used for the indentation. Indentation mesh was used as shown in figure 4.3. The geometry of specimen was 2520nm length, 2520nm width, and 1080nm height. The geometry was set to that the boundary effects are negligible to the results used for this finite element calculation.

At the bottom of the body, the four nodees at the corner were constrained so that the displacement does not occur in x,y, or z direction. For the tip, x and y directional displacement and rotation in all directions were constrained.

The stress was evaluated at the step where the reaction force on the tip was the closest from the nanoindentation experiment average pop-in load for each grain. Since the stress tensor of each element inside a single grain is expressed in crystal coordinate system, resolved shear stresses τ^R for {1 1 1}<1 1 2> partial dislocation slip systems(Table 4.3) for FCC material were calculated by

$$\tau^R = [\boldsymbol{Q}^T \boldsymbol{\sigma}^C \boldsymbol{Q}]_{12} \qquad \text{(Equation. 4.56)}$$

where $\boldsymbol{Q}$ is the rotation matrix,

$$\boldsymbol{Q} = \begin{pmatrix} 1/\sqrt{6} & 1/\sqrt{6} & -2/\sqrt{6} \\ -1/\sqrt{2} & 1/\sqrt{2} & 0 \\ 1/\sqrt{3} & 1/\sqrt{3} & 1/\sqrt{3} \end{pmatrix}$$

which transforms the coordinate system so that $\boldsymbol{x_1}'$ and $\boldsymbol{x_2}'$ is the slip plane normal and slip direction vector, respectively.

or the resolved shear stress can also be calculated by adopting Schmid tensor $\boldsymbol{\alpha}$.

$$\tau^R = \alpha_{ij}\sigma_{ij}^C \qquad \text{(Equation. 4.57)}$$

where $\boldsymbol{\alpha} = \frac{1}{2}(\boldsymbol{n} \otimes \boldsymbol{s} + \boldsymbol{s} \otimes \boldsymbol{n})$, while $\boldsymbol{n}$ and $\boldsymbol{s}$ are slip plane normal and slip direction vector, respectively.

After the calculation of resolved shear stresses of all elements, the maximum shear stress at slip system was found and upper 1%

values were also found to confirm that the maximum values are in reasonable area of the deformed body.

Table 4.2 Grain number and orientation data

Name	Euler angle (φ1,Φ,φ2)	Indentation plane index	Grain number
O1	(264, 27, 100)	(0.45 , -0.08, 0.89)	8, 18
O2	(147,30, 174)	(0.05, -0.50, 0.87)	78, 80
O3	(46,48, 318)	(-0.49, 0.55, 0.67)	65
O4	(156, 44, 204)	(-0.28, -0.6, 0.72)	127

Table 4.3 Shockley partial dislocation slip systems of FCC materials.

slip plane	**slip direction**
(1 1 1)	[1 1 -2]
	[1 -2 1]
	[-2 1 1]
(1 1 −1)	[1 1 2]
	[-1 2 1]
	[2 -1 1]
(1 −1 1)	[-1 1 2]
	[1 2 1]
	[2 1 -1]
(-1 1 1)	[1 -1 2]
	[1 2 -1]
	[2 1 1]

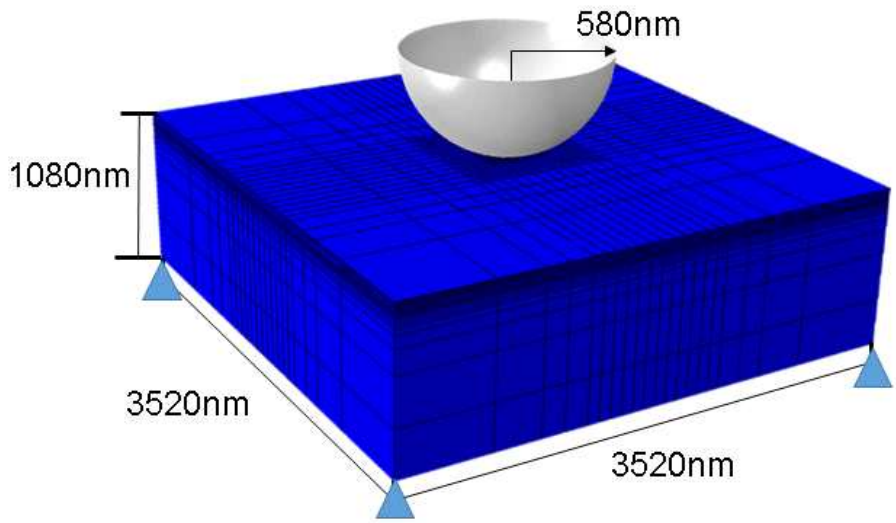

Figure 4.3 Mesh used in finite element calculation to simulate nanoindentation.

5. Results and Discussion

5.1 Elastic Energy of Circular Dislocation Loop in Anisotropic Medium

Elastic energy of a circular dislocation loop was based on the equation derived by Chu et al[40]. The parameters used can be seen in table 4.1. The Burgers vector of the dislocation loop was thought as Shockley partial dislocations of FCC crystal structure,in this calculation, a/6[1 1 −2], with dislocation loop plane of (1 1 1), the close-packed plane. In this study, only circular dislocation loops were considered, thus aspect ratio was not varied but set as 1.

Figure 5.1 Show the results of elastic energy vs dislocation loop radius. For comparison, the energy calculated with isotropic condition were also plotted. It can be seen that the consideration of anisotropy caused the elastic energy of a dislocation loop to be decreased.

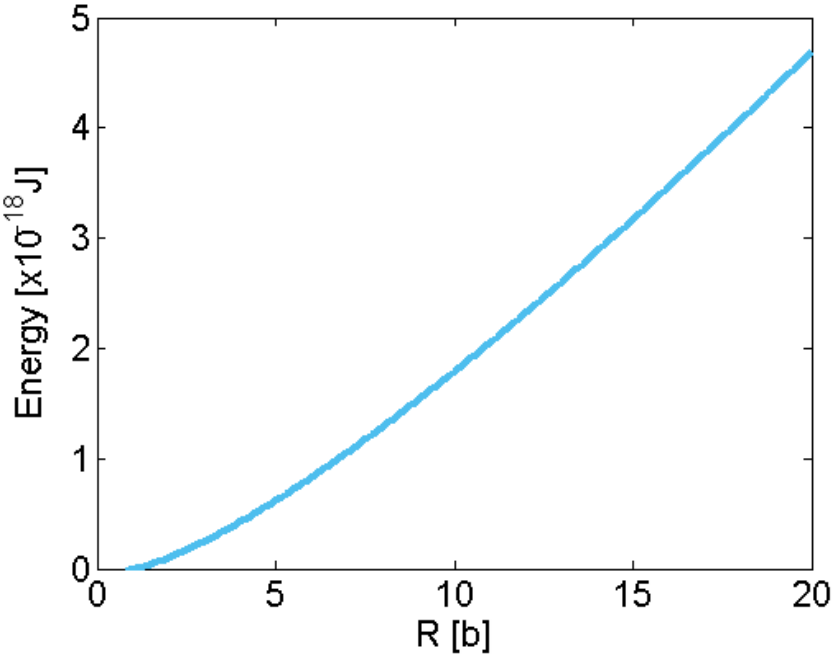

Figure 5.1 Elastic energy vs dislocation loop radius, for Cu

5.2 Maximum Shear Stress at Dislocation Nucleation

5.2.1 Nanoindentation and Electron Backscatter Diffraction

Load-displacemetn curves (LD curves) were obtained by nanoindentation, and number of pop-ins were observed. With EBSD analysis, orientations of the grains indented were identified and whether the indentation was done on grain interior, instead of grain boundaries, were confirmed.

Figure 5.2 shows the EBSD x3-directional mapping for indented surface of Cu. 4 different orientations were selected to obtain the strength of dislocation nucleation by nanoindentation. The grains were selected so that there were enough number of indents to be analyzed. Grain numbers 18 and 8, and 80 and 78 have similar orientation, Euler angle of [264.665, 27.269, 100.03]and [264.625, 27.199, 100.03], and [147.505, 29.797, 173.74] and [147.451, 29.919, 173.76], respectively. So those grains were regarded as same orientation to increase the sample number for accuracy. The Euler angles and indentation plane indices of each grain are listed in table 4.2, with nominations for each orientation that will be used through this paper.

Figure5.3 shows the load-displacement graphs of each orientation. It can be seen that the burst of displacement, pop-ins, are distributed along different loads. This is because the nanoindentation

results are very sensitive to surface conditions and dislocation status.

By plotting the cumulative probability of pop-in loads of each orientation, it can be seen that the pop-in loads are distributed as S-curve shape(Figure 5.4). The representative pop-in loads for each orientation of the grains indented were chosen as the average of each pop-in load, and the average values and standard deviations are listed in table 5.1.

Table 5.1 average pop-in loads and standard deviations of each grain.

	O1	O2	O3	O4
average pop-in load [μN]	125.73	136.43	104.45	123.58
standard deviation	47.5	53.5	48.6	41.8

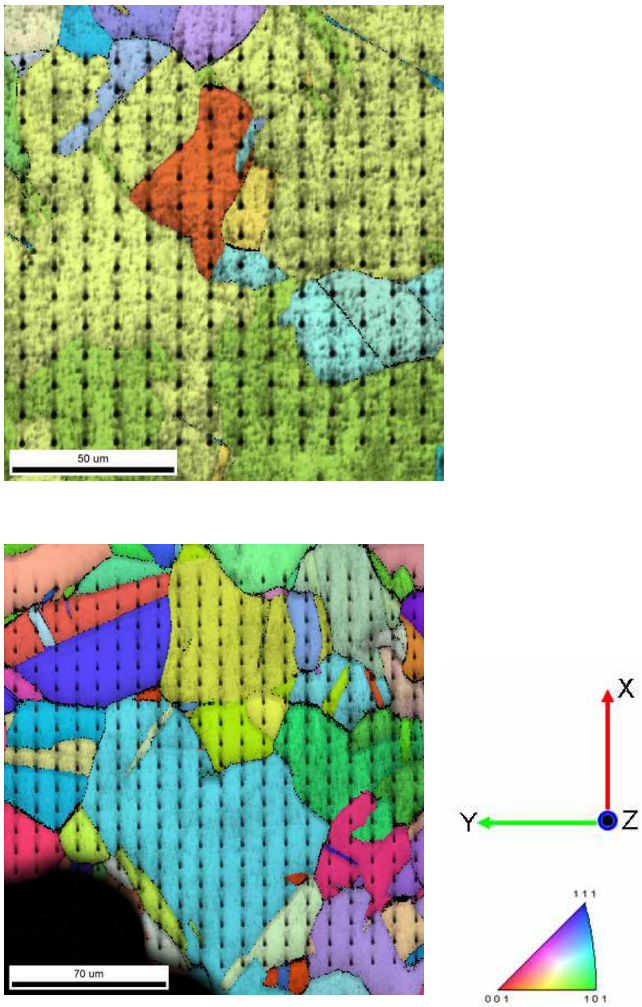

Figure 5.2 z directional EBSD inverse pole figure map

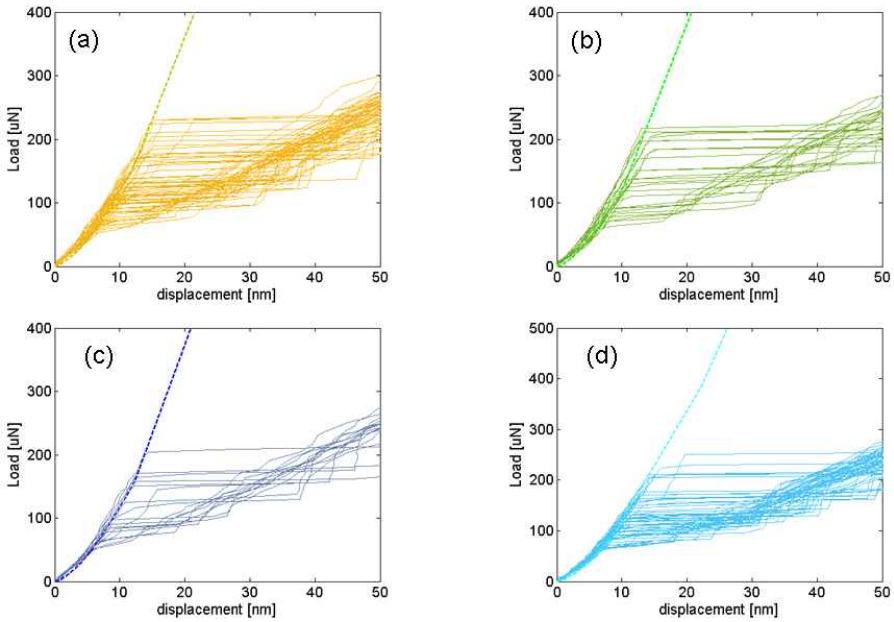

Figure 5.3 LD curves for 4 different orientations. (a), (b), (c), and (d) are for O1, O2, O3, and O4, respectively.

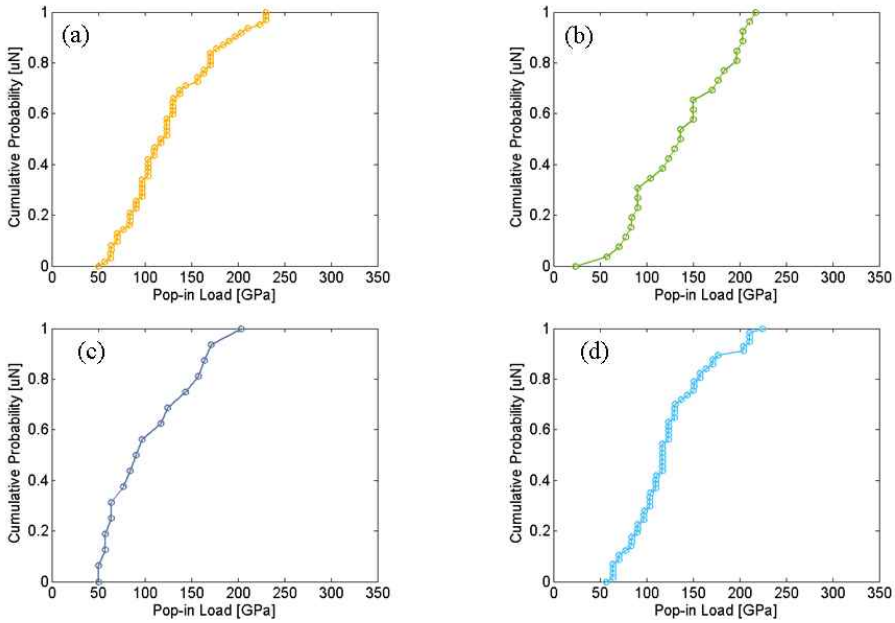

Figure 5.4 cumulative probability of pop-in loads.(a), (b), (c), and (d) are for O1, O2, O3, and O4, respectively.

5.2.2 Finite Element Calculation

Finite element calculations were done to simulate the nanoindentation of differently oriented grains, and analyze the resolved shear stresses of at dislocation nucleation when pop-in occurs.

Figure 5.5 shows the load-displacement results of nanoindentation FE calculation. Since the calculations were done only considering elastic deformation, the shape of LD curves are similar to that of the experimental data at early-stage deformation, where the deformation is elastic and load is proportional to $(\text{displacement})^{1.5}$.

Figures 5.6-5.9 and 5.10-5.13 show stress and strain fields underneath the indenter tip, respectively for each of the orientations.

To obtain the stress values at the load where pop-in occurred, stress tensor values were selected at the step where the load by FE analysis reached the load of pop-in from indentation experimental data, stated in table 5.2, for each orientation.

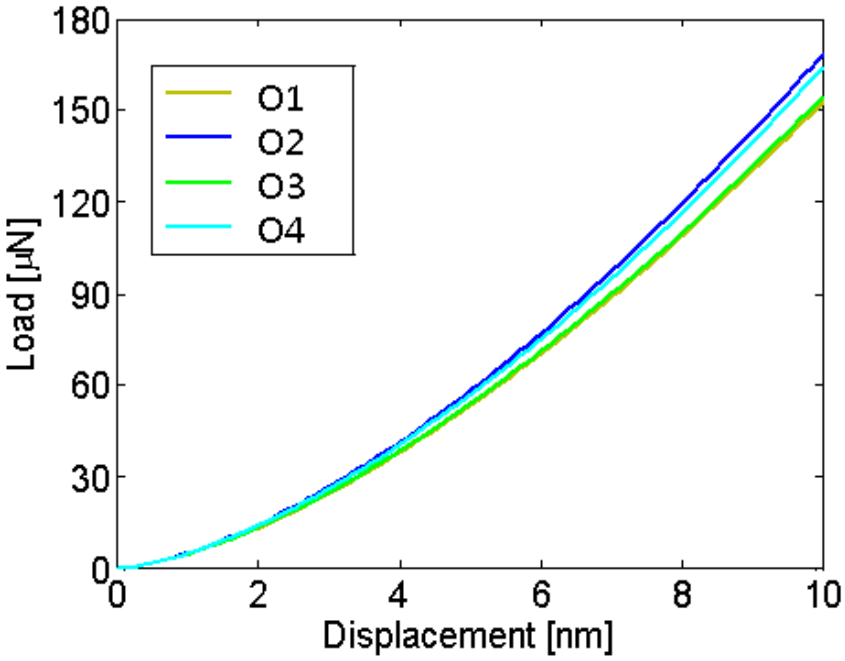

Figure 5.5 Load-displacement curves of each orientation.

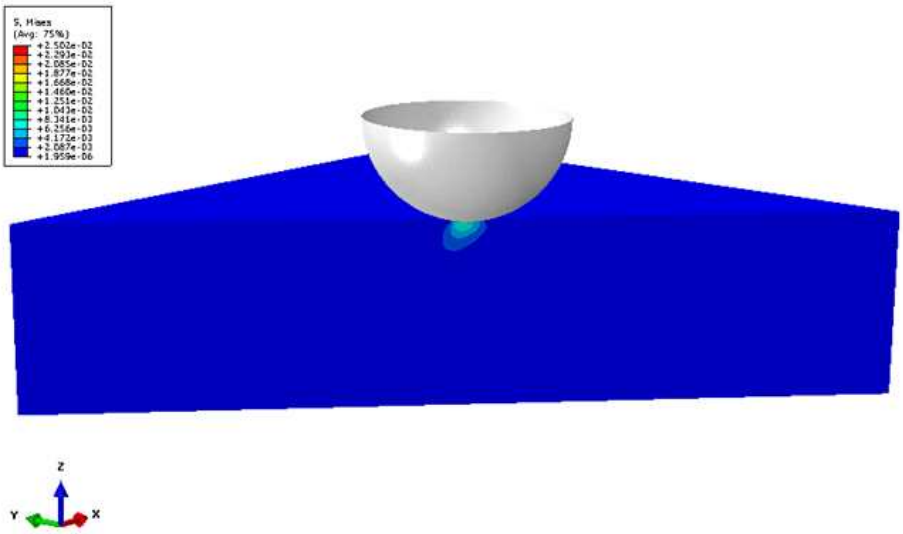

Figure 5.6 Stress fields of O1

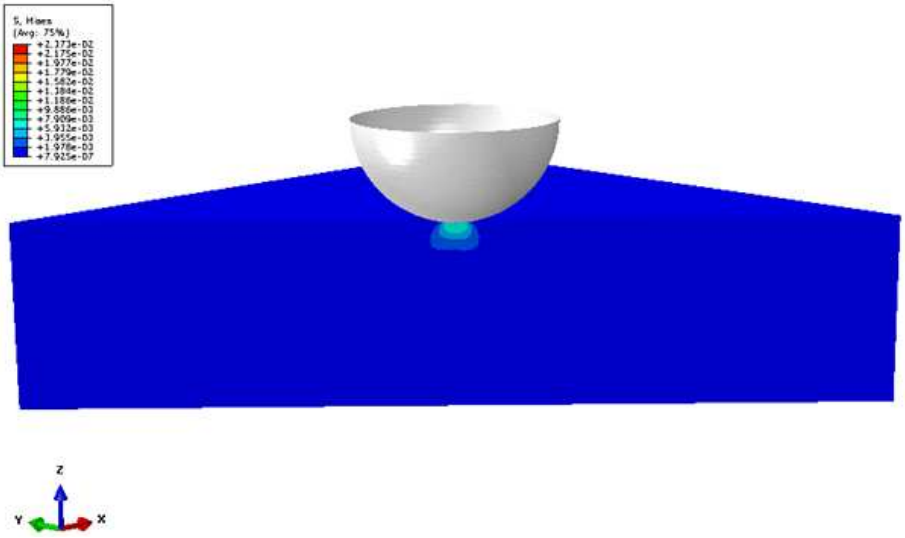

Figure 5.7 Stress fields of O2

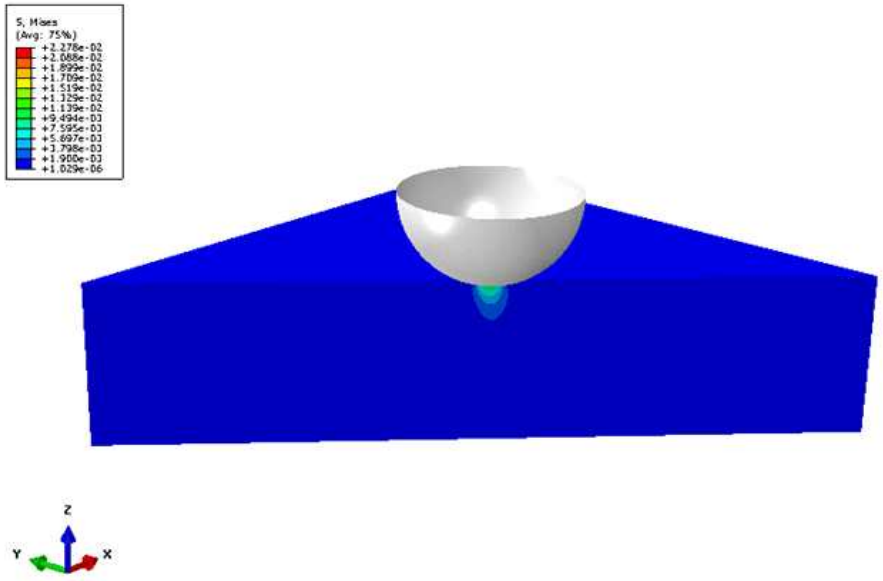

Figure 5.8 Stress fields of O3

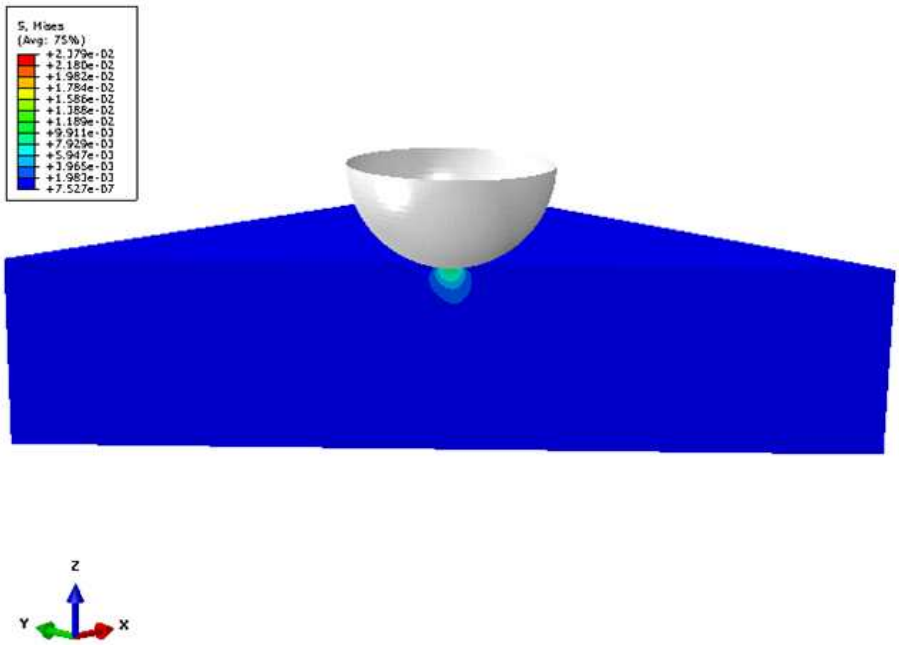

Figure 5.9 Stress fields of O4

5.2.3 Calculation of Maximum Shear Stress at Dislocation Nucleation

With the results from FE calculation of nanoindentation, stress tensors of each element on specimen could be obtained at the load when pop-in occurred. The stress tensors obtained were base on the crystal coordinate system. To find the resolved shear stresses for the partial dislocation slip systems of FCC material, Schmid tensor, mentioned in section 4.2 were used for all possible slip systems. Of all the resolved shear stresses, for all slip systems and all elements, the maximum values were chosen. To verify whether mesh affected the results, maximum values of upper 1% were selected to make sure that the maximum values determined were on that area of the specimen, confirming the maximum values were not induced by a numerical error.

Table 5.3 are the maximum resolved shear stresses of each orientation and their corresponding slip systems that were likely to be activated. Figure 5.14 show the position of the maximum resolved shear stress, and the region of upper 1% resolved shear stress values of all elements. Figures 5.15-5.17 show the results from the other orientations. Note that for O1-O3, the upper 1% of resolved shear stresses are distributed into 2 different slip systems. The slip systems where the maximum shear stresses had about 0.1 GPa higher than the other slip system's maximum resolved shear stresses. It can be thought that both

slip systems are likely to be activated because there might be some intrinsic defects or surface roughness that can affect the stress fields. For O4, only one slip system was possible of activating.

The obtained values of maximum shear stress acting on partial dislocation slip systems were in range of G/15, which is known to be the theoretical strength of dislocation nucleation. From this results, it can be confirmed that the pop-ins observed during nanoindentation was a sign of incipient plasticity by dislocation nucleation rather than movement of pre-existing dislocation or activation of Frank-Read source.

Table 5.2 Maximum resolved shear stresses and their corresponding slip systems

	O1	O2	O3	O4
Dislocation nucleation strength [GPa]	3.11	3.24	3.06	3.34
slip plane	(1 1 1)	(1 -1 1)	(1 1 1)	(1 -1 1)
slip direction	[-1 2 -1]	[2 1 -1]	[2 -1 -1]	[2 1 -1]

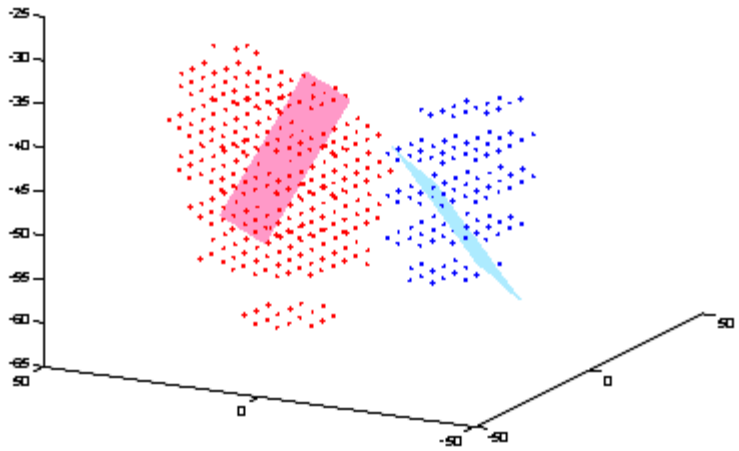

Figure 5.14 Position of maximum resolved shear stress and area of upper 1% values of the maximum value of O1 .

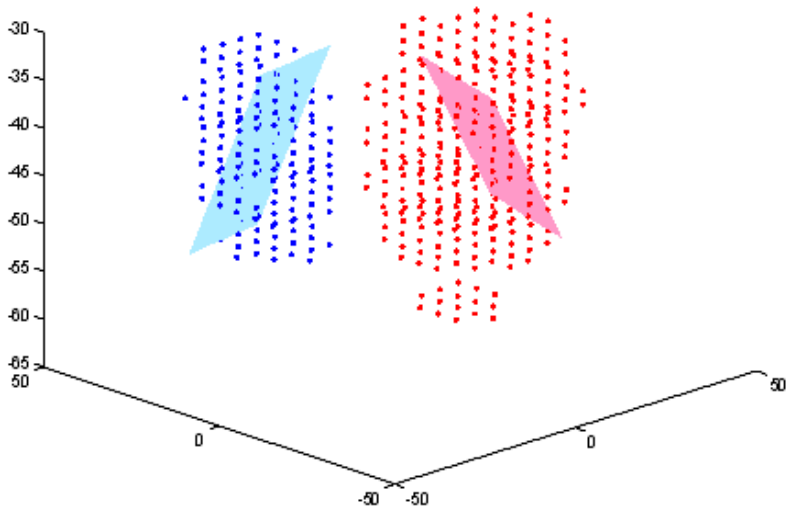

Figure 5.15 Position of maximum resolve shear stress and area of upper 1% values of the maximum value of O2 .

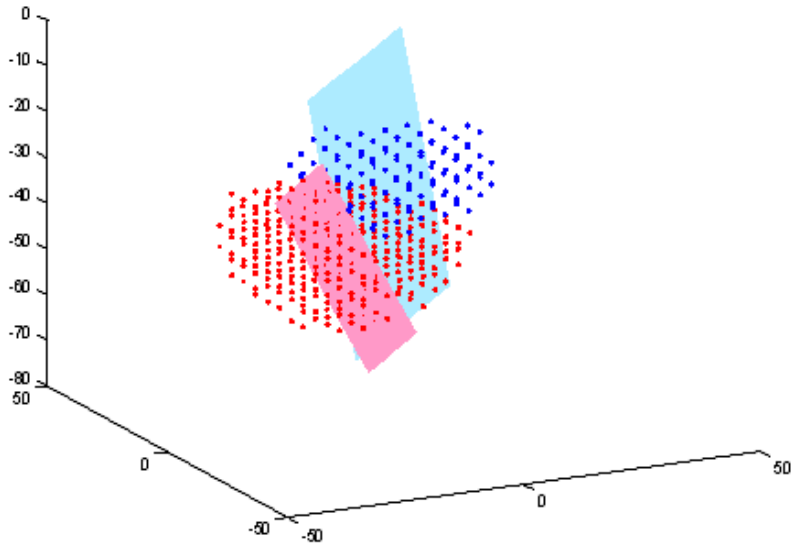

Figure 5.16 Position of maximum resolve shear stress and area of upper 1% values of the maximum value of O3 .

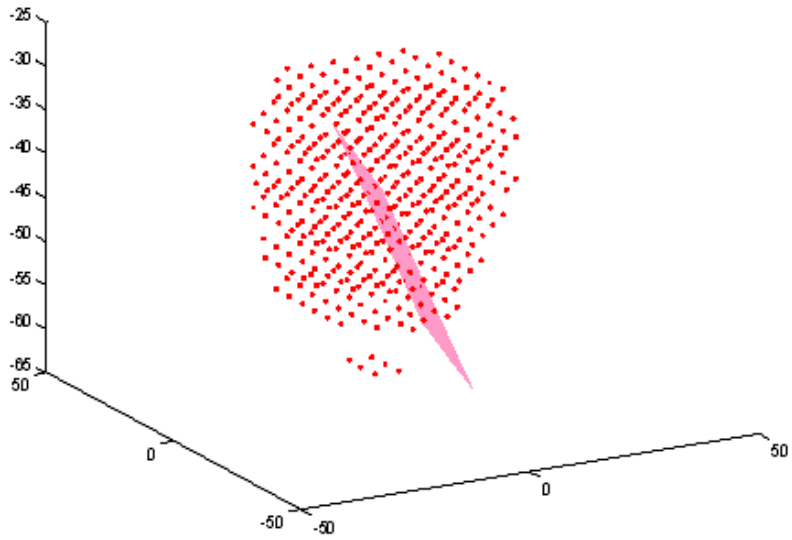

Figure 5.17 Position of maximum resolve shear stress and area of upper 1% values of the maximum value of O4 .

5.3 Dislocation Nucleation Energy in Anisotropic Medium and Evaluation of Stacking Fault Energy

By adoption of results from 5.1 and 5.2, the energy of a circular dislocation loop in isotropic medium can be modified as dislocation nucleation energy in anisotropic medium. Table 5.4 show the estimated stacking fault energies of each orientation. Ideally, stacking fault energy is independent of orientation, but difference in maximum shear stress at dislocation nucleation during nanoindentation caused such differences. With dislocation core radius of $\rho = 0.63b$, which is a resonable range of the parameter[6,10]. The stacking fault energy of Cu was estimated to be in the range of 42~83mJ/m^2, which was in the range of known stacking fault energy of Cu(40~80mJ/m^2)[40-42]. Figure 5.20 shows the energy of a circular dislocation loop in anisotropic medium, with stacking fault energy of 61mJ/m^2 and the energy barrier. Energy barrier reached 0 at the applied shear stress of 3.2GPa, which is the critical resolved shear stress obtained by nanoindentation experiment.

6. Conclusion

This study was carried out in order to investigate the dislocation nucleation behavior and stacking faults in FCC crystal, Cu, by means of nanoindentation. From the analytic equation of dislocation nucleation in isotropic medium, new method of evaluating stacking fault energy were suggested. Due to the limitations of the equation that it is an approximation in isotropic condition, each of the term constituting the equation(elastic energy, stacking fault energy, work done by shear stress) were investigated so that anisotropy was considered.

The elastic energy term was calculated based on other studies, and for the shear stress term, electron backscatter diffraction(EBSD) and finite element(FE) analysis were done to obtain the maximum resolved shear stress at dislocation nucleation for the specimen(Cu). The dislocation nucleation strength value were in the range of theoretical strength of dislocation nucleation(~G/15). With these results, the stacking fault energy were evaluated to be 61mJ/m^2, which is in the range of known stacking fault energy value of pure Cu.

The method of evaluating stacking fault energy with nanoindentation suggested in this study can be applied to wide range. It is relatively simple way of estimating SFE of various materials, less

time consuming than other current methods such as observation in TEM or using neutron diffraction, etc. Although it is difficult to obtain the exact value of SFE with this method, relative estimation and evaluation is possible with reasonable degree of error.

6. References

[1] Hirth JP, Lothe J. Theory of Dislocations. 2nded. NewYork: Wiley; 1982.

[2] Mura T. Micromechanics of Defects in Solids. 2nded. Dordrecht, Kluwer Academic Publishers; 1991.

[3] Gavazza SD, Barnett DM. J Mech Phys Solids 1976; 24:171.

[4] Kroner E. Egreb Angew Math 1958;5:163.

[5] de Wit R. Solid State Phys 1960;10:249.

[6] Cai W, Arsenlis A, Weinberger CR, Bulatov VV. J Mech Phys Solids 2006;561:587.

[7] Hull D, Bacon DJ. Introduction to Dislocations. 4thed. Oxford: Butterworth Heinmann; 2001.

[8] Courtney TH. Mechanical Behavior of Materials. 2nded. Singapore: McGraw-Hill; 2000.

[9] Dieter GE. Mechanical Metallurgy. Singapore: McGraw-Hill; 1988.

[10] Aubry S, Kang K, Ryu S, Cai W. Scripta Mater 2011; 1043:1046.

[11] Xu G, Argon AS. Philos Mag Lett 2000;605:611.

[12] de Koning M, Cai W, Bulatov VV, Phys Rev Lett 2003; 025503.

[13] Xu G, Nabarro FRN, Hirth JP. Dislocations in Solids. North Holland: Elsvier; 2004.

[14] Rabkin E, Nam HS, Srolovitz DJ. Acta Mater 2007; 2085:2099.

[15] Gutkin MY, Ovid'ko IA. Acta Mater 2008; 1642:1649.

[16] Xiang Y, Wei H, Ming P, Weinan E. Acta Mater 2008; 1447:1460.

[17] Lee TH, Shin E, Oh CS, Ha HH, Kim SJ. Acta Mater 2010; 3173:3186.

[18] L Remy, A Pineau. Mater Sci Eng 1976; 26:123.

[19] J Talonen, H Hanninen. Acta Mater 2007; 55:6108.

[20] F Lecroisey, APineau. Metall Trans 1972; 3:387.

[21] GB Olson, M Cohen. Metall Trans A 1976; 7:1897.

[22] RP Reed, RE Schramm. J Appl Phys 1974; 45:4705.

[23] Zhu T, Li J, Van Vilet KJ, Ogata S, Yip S, Suresh S. J Mech Phys Solids 2004; 691:724.

[24] Fang Q, Zhang L. J Mater Res 2013; 1995:2003.

[25] Michalske TA, Houston JE. Acta Mater 1998; 391:396.

[26] Bei H, Gao YF, Shim S, George EP, Pharr GM, Phys Rev B 2008; 060103.

[27] Schuh CA, Lund AC. J Mater Res 2004; 2152:2158.

[28] Lilleodden ET, Zimmerman JA, Foiles SM, Nix WD. J Mech Phys of Solids 2003; 901:920.

[29] Chang HJ, Han HN, Fivel MC. Key Eng Mater 2007; 925:930

[30] Ahn TH, Oh CS, Lee K, George EP, Han HN. J Mater Res 2012; 39:44.

[31] Shin JH, Kim SH, Ha TK, Oh KH, Choi IS, Han HN. Scripta Mater 2013; 483:486.

[32] Lee K, Park SJ, Choi YS, Kim SJ, Lee TH, Oh KH, Han HN. Scripta Mater 2013; 618:621.

[33] Rohatgi A, Vecchio KS, Gray III GT. Metall Mater Trans A 1999; 135:145.

[34] Lu Gang, Kioussis N, Bulatov VV, Kaxiras E. Phys Rev A 2000; 3099:3108.

[35] Zimmerman JA, Gao H, Abraham FF. Modelling Simul Mater Sci Eng 2000; 103:115.

[36] Johnson KL. Contact Mechanics. Cambridge: Cambridge University Press; 1999.

[37] Oliver WC, Pharr GM. J Mater Res 1992;1564:1583.

[38] Jeong SM, Shum PW, Shen YG, Li KY, Mai YW, Lee HL. Jpn J Appl Phys 2006; 6411:6416.

[39] Mao WG, Shen YG, Liu C, Euro J. Ceram Soc 2011; 1865:1871.

[40] Chu HJ, Wang J, Zhou CZ, Beyerlein IJ. Acta Mater 2011; 7114:7124.

[41] Zhao YH, Zhu YT, Liao XZ, Horita Z, Langdon TG. Mater Sci Eng A 2007; 22:26.

[42] Stobbs WM, Sworn CH. Phil Mag 1971; 1365:1371.

국문 초록

적층결함에너지(SFE)는 부분 전위의 발생으로 인해 생성되는 적층결함의 단위 면적당 에너지로 구조 재료에 있어 매우 중요한 역할을 하는 물성이다. 이러한 적층결함에너지를 구하기 위한 새로운 방식으로 나노압입실험과 전위 생성에 따른 에너지 변화 대한 해석적 식을 활용하였다. 그러나 기존의 식은 재료의 등방성을 가정하였기 때문에 이러한 한계를 보완하고자 이방성을 고려하기 위한 연구를 진행하였다.

전위 생성에 따른 에너지 식에 포함되는 전위 자체의 탄성에너지의 이방성을 고려하기 위해서 기존에 알려져 있는 이방성을 고려한 연구를 참고하였다. 또한 전위생성에너지 식에 사용되는 전위 생성시의 전단응력은 나노압입실험, 후방산란전자 회절(EBSD) 분석, 유한요소(FE) 해석을 활용하여 부분전위 슬립계에 작용하는 전단응력의 최댓값을 구하였다. 구해진 전단응력 값은 기존에 알려져 있는 재료의 이론적 강도와 수준으로 나타났으며 위의 결과를 종합하여 구한 적층결함에너지 역시 기존에 알려진 값과 유사하게 평가되었다.

핵심어: 적층결함에너지, 나노압입실험, 전위 생성, 전위 에너지 배리어, 이방성

Student number: 2014-21477